Generalized Phase Diagram for Microphase-Separated Systems and Its Determination by Small-Angle Scattering

Marc André Micha, Christian Burger,* and Markus Antonietti

Max-Planck-Institut für Kolloid- und Grenzflächenforschung, Kantstrasse 55, D-14513 Teltow-Seehof, Germany

Received January 22, 1998
Revised Manuscript Received May 22, 1998

Introduction. A large variety of polymeric materials, e.g., block copolymers, interpenetrating polymer networks, or complexes of polyelectrolytes with surfactants or lipids, form well-defined microphase-separated structures. The geometry and architecture of these mesophases is controlled by several parameters such as the volume fraction, the interface energy, and local molecular packing effects.

While detailed theoretical descriptions are found for block copolymers[1−4] little is known about the phase behavior of strongly segregated systems. The morphology of such materials is difficult to predict, and empirical approaches govern the field.

A powerful technique for the study of the microphase-separated structures is small-angle scattering (SAS). If highly ordered mesophases with large macrolattices are present, a sufficiently large number of Bragg reflections are observed, which permit a structure determination using classical crystallographic methods. Frequently, however, the number of observable Bragg reflections is low and the line profiles overlap heavily so that crystallographic methods are not applicable.

In this communication, we report a new method of SAS data evaluation for two-phase systems with sufficiently strong segregation that is applicable to a wide range of mesophase morphologies and states of order. The method permits the determination of the type of mesophase morphology even in the case where only a single SAS peak is observable. The theoretical approach developed for this purpose results in a generalized phase diagram based on purely geometrical quantities determined from the total intensity distribution of the SAS.

Porod's Law. Consider a sample of irradiated volume V containing a spatial distribution of two microphases of constant densities ρ_1 and ρ_2, respectively. In the case of small-angle X-ray scattering (SAXS) the ρ_i are the electron densities, and in the case of small-angle neutron scattering (SANS) the scattering length densities, respectively. The interfacial boundary is assumed to be infinitely sharp.

The asymptotic behavior of the SAS from such a two-phase system is described by Porod's law.[5] For pinhole collimation it is given by

$$I(s) = \frac{k}{2\pi^3 l_p s^4} + O(s^{-6}) \tag{1}$$

where $s = 2\lambda^{-1} \sin\theta$ is the absolute value of the scattering vector, l_p is Porod's length (see below), and k is Porod's invariant,

$$k = \int I(s)\, \mathrm{d}^3 s = V(\rho_1 - \rho_2)^2 \phi(1-\phi) \tag{2}$$

where ϕ is the volume fraction of one microphase. In the following, we will take k to be unity.

l_p is related to the specific interface of the two-phase system.

$$l_p = 4\phi(1-\phi)\frac{V}{S} \tag{3}$$

where S is the total interfacial area in the irradiated volume.

3D Fourier transformation of (1) leads to the real space form of Porod's law

$$\gamma(r) = 1 - \frac{r}{l_p} + O(r^2) \tag{4}$$

where $\gamma(r)$ is the normalized electron density autocorrelation function or characteristic function.[5]

Kirste−Porod Law. Kirste and Porod[6] have shown that the asymptotic behavior in $I(s)$ and the corresponding series development of $\gamma(r)$ is related to the curvature of the interface. In real space we have

$$\gamma(r) = 1 - \frac{1}{l_p} r + \frac{b}{l_p} r^3 + O(r^5) \tag{5}$$

A quadratic term is only present if the interface contains sharp edges.[6,7] Since the morphologies considered in this paper are expected to have continuously smooth interfaces, this term can be omitted.

The parameter b as given by Kirste and Porod depends on averages of the interface curvature defined by

$$b = \frac{1}{12}\overline{c_1 c_2} + \frac{1}{32}\overline{(c_1 - c_2)^2} \tag{6}$$

where c_1 and c_2 are the two principal curvatures[8] in every point of the interface and $\overline{(...)} = \langle ... \rangle_S$ denotes averaging over the total interface.

For convenience, we rewrite (6) in the following way

$$b = \frac{1}{32}\overline{(c_1 + c_2)^2} - \frac{1}{24}\overline{c_1 c_2} = \frac{1}{8}\left(\overline{H^2} - \frac{1}{3}\bar{K}\right) \tag{7}$$

which demonstrates more clearly in which way the curvature parameter b is related to the averages over the squared mean curvature $H^2 = (c_1 + c_2)^2/4$ and the Gaussian curvature $K = c_1 c_2$.[8]

Transformation to reciprocal space leads to the asymptotic behavior of the scattering curve including the curvature parameter

$$I(s) = \frac{1}{2\pi^3 l_p s^4}\left(1 + \frac{3b}{\pi^2} s^{-2} + O(s^{-4})\right) \tag{8}$$

or, for the case of Kratky collimation in the infinite slit approximation

$$J(s) = \frac{1}{4\pi^2 l_p s^3}\left(1 + \frac{9b}{4\pi^2} s^{-2} + O(s^{-4})\right) \tag{9}$$

* To whom correspondence should be addressed.

S0024-9297(98)00085-0 CCC: $15.00
Published on Web 08/01/1998

If the two-phase system is built up of essentially monodisperse structural units, additional oscillating terms will be present in (8) and (9).

Reduced Parameters. To eliminate the dependence on actual length scales, let us introduce reduced parameters by measuring all lengths in units of the period $L = 1/s^*$ determined by the position of the most pronounced intensity maximum s^* in the SAS curve.

$$\iota = \frac{S}{V}L \tag{10}$$

$$\kappa = \langle H^2 \rangle_S^{1/2} L \tag{11}$$

It is seen from (3) that the reduced specific interface ι (iota) is related to Porod's length l_p. In the lamellar case it corresponds, apart from a constant factor of 2, to the planarity parameter S/S_0 introduced by Perret and Ruland .[9] The additional normalization to unity in the unperturbed case is not performed here in order to allow comparisons between different morphologies. The reduced root-mean-square (rms) mean curvature κ can be extracted from the mean curvature part of the curvature parameter b in (7). The separation of b into its two components will be discussed below.

$\kappa-\iota$ Phase Diagram. Using the reduced parameters κ and ι defined above, we are now able to construct a general phase diagram for two-phase systems. κ is taken as the abscissa and ι as the ordinate of a plot allocating the different phase morphologies. With increasing curvature parameter, the structures are more and more bent, and we expect the classical sequence of lamellae → cylinders → spheres to occur with increasing κ. For block copolymers, κ thus replaces the asymmetry of the volume fraction $|\phi - 0.5|$ as the geometrically determining parameter of the phase diagram. In the case of constant mean curvature (CMC) surfaces, κ corresponds to the spontaneous curvature c_0 (in our reduced normalization) of the interface.

The interface parameter ι describes the relative amount of interface and represents, in a first approximation, an energy scale: for systems where the interface energy represents the predominant driving force, ι will adopt the lowest possible value. Deviations from this behavior show that other energy contributions become significant.

For most known mesophase morphologies it is straightforward to calculate κ and ι as a function of the volume fraction ϕ by simple geometrical considerations. Figure 1 shows such a theoretical phase diagram where the lamellar and cylindrical morphologies (including their undulated derivatives), the gyroid phase[10,11] as well as various disperse phases (e.g., spherical cubic, prolates, and oblates) have been considered.

Due to the normalization, plain lamellae produce a single point at $\kappa = 0$ (no undulations) and $\iota = 2$ (two interfaces AB and BA per period). When undulations start to grow on the surface (mattress phases), both the curvature and the interface increase. Various special cases based on 1D or 2D sine wave undulations can be treated analytically and cover the corresponding regions of the phase diagram for undulated lamellae.

For mattress phase's ι rises with increasing κ, while for cylindrical and disperse morphologies a reciprocal behavior is observed. The disperse domain is found at κ higher than that of the cylindrical domain, while the line indicating the gyroid phase links the cylindrical and the lamellar domain. A region of perforated layers with catenoid-shaped holes is expected in the vicinity of the gyroid phase. However, since the perforated layer phase has a large number of adjustable parameters, the corresponding region in the phase diagram is not well-defined.

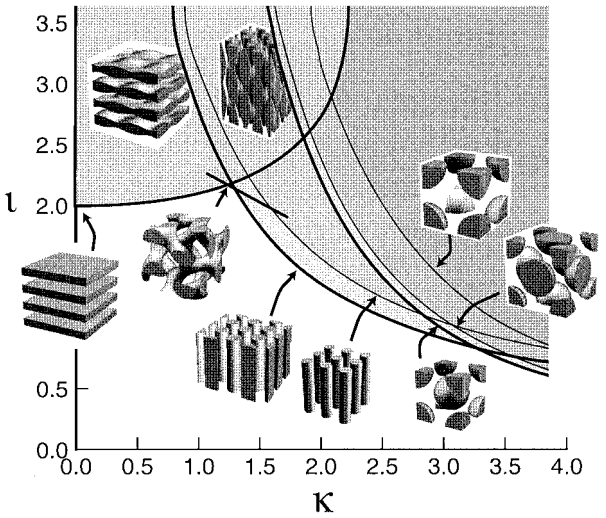

Figure 1. The $\kappa-\iota$ diagram for lamellae, cylinders, spheres, and the $Ia\bar{3}d$ double gyroid. The lines represent the undeformed phases. Rippled, undulated, or otherwise deformed phases are found in the shaded regions above and to the right of the corresponding lines.

Already at this stage it can be seen that a classification in accordance with the $\kappa-\iota$ diagram allows a generic prediction of phase transitions in systems driven by interface energies. The spontaneous curvature can be regarded as a driving parameter, and a phase transition to a new structure will occur when a new region with a similar κ but a lower ι can be reached in the vicinity of the phase diagram.

It should be noted that for increasing curvature this theoretical scheme predicts the sequence lamellae → undulated lamellae → gyroid → hexagonally packed cylinders → BCC spherical, i.e., the sequence found for block copolymers.

Other morphologies such as the highly undulated structures described for polyelectrolyte surfactant complexes[12] can occur when additional energy contributions besides the bending and interface energies become significant. The importance of these additional contributions is mainly based on the molecular packing and the local geometry.

Practical Implementation of the Method. The direct determination of Porod's length l_p and especially the curvature parameter b from SAS curves based on (8) or its slit-smeared equivalent (9) can be heavily affected by interdomain and intradomain interferences that produce maxima and oscillations in the scattering curve. Furthermore, the effects of the finite thickness of the interfacial boundaries[16] and of density fluctuations in the bulk domains[17] have to be taken into account.

To overcome these problems, a method has been developed to determine the parameters from the correlation function $\gamma(r)$. In real space the maxima of the scattering curve are transformed into density oscillations and scattering curve oscillations lead to singularities at a finite distance from the origin. Both effects do not influence the expansion (5) of the correlation function at small r.

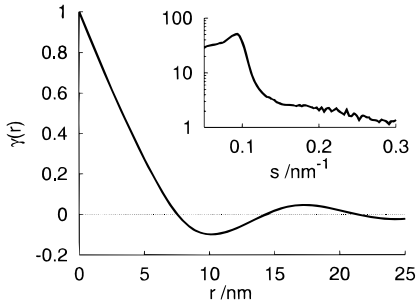

Figure 2. Scattering curve (inset) and characteristic function $\gamma(r)$ of a strongly segregated block copolymer with perfluorinated side chains showing a hexagonal mesophase.

An effective method to calculate $\gamma(r)$ with the necessary precision has been developed, which is based on an expansion of $I(s)$ into generalized Laguerre orthogonal functions. The method, which is also applicable in the case of finite slit Kratky collimation, will be described in detail elsewhere.[13] The parameters l_p and b are obtained by direct fitting of the transformed experimental data to (5). If necessary, the effect of the cutoff of the scattering curve at large values of s can be eliminated by suitable corrections.

It should be noted that an extremely strong segregation of the two-phase system is not necessary for the applicability of the approach. As long as the interfacial width is small compared to Porod's length l_p, its effects can usually be taken into account and eliminated. However, as the number of corrections to the original data increase, the accuracy of the scattering data and the reliability of the data treatment techniques become more important.

Application to Experimental Data. As model systems for checking the applicability of the method we used samples of diblock copolymers of polystyrene and 1,2-polybutadiene where perfluorinated side chains of varying lengths have been grafted to the olefin double bonds of the butadiene block.[14] We are thus dealing with two-phase systems consisting of aryl and perfluorinated domains that are strongly incompatible. This leads to a sharp density step in the interface so that the effect of a finite width of the interfacial boundary can be neglected. In addition, we applied the method to SAXS curves from unsubstituted polystyrene-*b*-polybutadiene and polyisoprene block copolymers measured by Wolff,[15] taking into account corrections for the finite interface width[16] and the coarseness and interdigitation of the interface.[18,19] In all cases, the background due to density fluctuations in the bulk has been taken into account.[17]

Figure 2 (inset) shows the SAXS curve measured in Kratky collimation from a polystyrene-*b*-poly(vinylperfluorooctanic ester). An intense first-order maximum is clearly visible. Higher order maxima cannot be separated unambiguously so that a definite type of morphology cannot be assigned by classical techniques.

Applying the transformation to real space produces the normalized autocorrelation function shown in Figure 2 from which Porod's length l_p and the curvature parameter b can be extracted. Converting these parameters to the reduced parameters ι and κ (with the assumption $\bar{K} = 0$, see the discussion below) leads to the point in the $\kappa-\iota$ diagram marked with an arrow in Figure 3. The position of this point in the $\kappa-\iota$ diagram strongly suggests the presence of hexagonally packed cylinders, a finding that was subsequently confirmed by transmission electron microscopy.

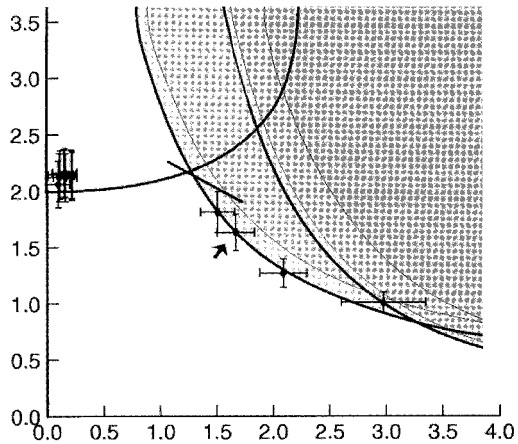

Figure 3. The $\kappa-\iota$ diagram filled with experimental data points obtained from various block copolymer samples.

The phase diagram Figure 3 contains various further data points obtained for block copolymers, all allowing an unambiguous structure assignment to a lamellar or hexagonal phase. All data points closely follow a curve of minimal interface ι, i.e., the mesophase formation of block copolymers is, as expected, only driven by interface and curvature effects. This behavior allows an unambiguous assignment of a distinct phase morphology to all examined samples, which cannot be easily accomplished by other techniques.

It is of interest to note that many samples included in Figure 3 were not extensively annealed so that the perfection and the size of the macrolattices was low. Consequently, the SAXS curves contained, in most cases, only one prominent peak. It is obvious that under these circumstances a classical structure determination is not possible.

Despite this difficulty, the $\kappa-\iota$ approach leads to well-defined coordinates in the phase diagram which permit, in most cases, a definite structure proposal. It should be noted that the curvature is a spatially confined property of the interface that is completely independent of long-range order. Thus, the annealing of distorted macrolattices has, in general, only little effect on the total interface ι and the rms mean curvature κ. Consequently, a structure assignment based on the $\kappa-\iota$ diagram is much less affected by disorder than assignments based on classical methods of crystallography or electron microscopy.

Furthermore, it should be pointed out that for sample coordinates in the $\kappa-\iota$ diagram that do not coincide with the line of minimal interface area it is possible to obtain not only an estimate of the basic morphology but also a qualitative or semiquantitative description of the kind of distortions present.

Analysis of the Kirste−Porod Curvature Parameter *b*. As can be seen from its definition (7), the Kirste-Porod curvature parameter b consists of a sum of two contributions, namely, an average over the squared mean curvature H^2 and an average over the Gaussian curvature K, respectively. Since only the rms mean curvature $(\overline{H^2})^{1/2}$ enters into our definition (11) of the reduced curvature parameter κ, the question about the separation of b into its two components arises.

Fortunately, the possible values $\bar{K}$ can assume are severely limited by the Gauss−Bonnet theorem of

differential geometry,[8] which states that the average of the Gaussian curvature K over a surface S is related to its topology:

$$\bar{K} = \langle K \rangle_S = \frac{\int\int K \, dS}{\int\int dS} = \frac{4\pi(1 - G)}{S} \qquad (12)$$

The genus G of the surface is an integer number depending on the topology only. It is invariant under distortions such as undulations or deformations, as long as the coherence of the surface is not affected.

In particular, it should be noted that $\bar{K}$ vanishes for lamellae and cylinders since at least one of the principal curvatures c_i is zero. Due to the Gauss−Bonnet theorem $\bar{K}$ remains zero for arbitrarily undulated lamellar and cylindrical phases as long as the topology does not change, e.g., as long as the lamellae are free of holes. In the case of nonvanishing $\bar{K}$, as in cubic structures or perforated lamellae, the value of $\bar{K}$ is limited to a finite set of discrete values since the genus G is an integer number. Such structures were not treated in the present work, but a more detailed discussion is found in ref 20.

Conclusion and Outlook. The determination of the specific interface area and the rms mean curvature from SAS measurements has been shown to be a powerful way of identifying morphologies in microphase-separated polymeric materials. The concept of the phase diagram using the newly introduced reduced parameters κ and ι is suitable for a quantitative interpretation of the experimental data.

The evaluation of SAS in terms of κ and ι is applicable not only to samples showing a number of Bragg reflections but also to weakly ordered or distorted systems, providing information about the basic morphology and, in some cases, the kind of distortion. Since longe-range order is not necessary the approach can also be applied to spongelike structures or similar disordered networks, provided a characteristic length scale L is found for the renormalization.

The $\kappa-\iota$ diagram developed appears to be valid for a large number of two-phase systems with sufficiently strong segregation. A classification of the relevant energy contributions to the mesophase formation becomes possible and, for special cases, predictions of phase stability can be made.

Acknowledgment. Thanks are due to Dr. S. Oestreich for providing the fluorinated block copolymer samples and to Dr. T. Wolff for the SAXS curves from the PS−PB and PS−PI block copolymers. C.B. wishes to thank Prof. W. Ruland for helpful discussions. Financial support by the Deutsche Forschungs-Gemeinschaft and the Max-Planck-Gesellschaft is gratefully acknowledged.

References and Notes

(1) Leibler, L. *Macromolecules* **1980**, *13*, 1602.
(2) Fredrickson, G. H.; Helfand, E. *J. Chem. Phys.* **1987**, *87*, 697.
(3) Helfand, E.; Wasserman, Z. In *Developments in Blockcopolymers*; Goodman, I., Ed.; Applied Science: New York, 1982.
(4) Semenov, A. N. *Sov. Phys. JETP* **1985**, *61*, 733.
(5) Porod, G. *Kolloid Z. Z. Polym*. **1951**, *124*, 83; **1952**; *125*, 51; **1952**, *125*, 108.
(6) Porod, G., Kirste, R. *Kolloid Z. Z. Polym*. **1962**, *184*, 1.
(7) Méring, J.; Tchoubar, D. *J. Appl. Crystallogr*. **1968**, *1*, 153; **1969**, *2*, 128.
(8) do Carmo, M. P. *Differential Geometry of Curves and Surfaces*; Prentice Hall: Englewood Cliffs, NJ, 1976.
(9) Perret, R.; Ruland, W. *Kolloid Z. Z. Polym*. **1971**, *247*, 835.
(10) Förster, S.; Khandpur, A. K.; Zhao, J.; Bates, F. S.; Hamley, I. W.; Ryan, A. J.; Bras, W. *Macromolecules* **1994**, *27*, 6922.
(11) Hajduk, D. A.; Harper, P. E.; Gruner, S. M.; Honeker, C. C.; Kim, G.; Thomas, E. L.; Fetters, L. J. *Macromolecules* **1994**, *27*, 4063.
(12) Antonietti, M.; Burger, C.; Effing, J. *Adv. Mater*. **1995**, *7*, 751.
(13) Burger, C.; Micha, M. A.; Ruland, W. Manuscript in preparation.
(14) Oestreich, S.; Antonietti, M.; Foerster, S.; Micha, M. A. *Acta Polym*. **1997**, *48*, 262.
(15) Wolff, T. Thesis, Marburg, 1994.
(16) Ruland, W. *J. Appl. Crystallogr*. **1971**, *4*, 70.
(17) Ruland, W. *Colloid Polym. Sci*. **1979**, *66*, 355.
(18) Ruland, W. *Macromolecules* **1987**, *20*, 87.
(19) Wolff, T.; Burger, C.; Ruland, W. *Macromolecules* **1994**, *27*, 3301.
(20) Micha, M. A. Thesis, Teltow, 1997.

MA980085C